Symmetry, equivalence, and molecular self-assembly

Kevin Van Workum* and Jack F. Douglas†
National Institute of Standards and Technology, Polymers Division, Gaithersburg, Maryland 20899, USA
(Received 14 October 2005; published 7 March 2006)

Molecular self-assembly at equilibrium is fundamental to the fields of biological self-organization, the development of novel environmentally responsive polymeric materials, and nanofabrication. Our approach to understanding the principles governing this process is inspired by existing models and measurements for the self-assembly of actin, tubulin, and the ubiquitous icosahedral shell structures of viral capsids. We introduce a family of simple potentials that give rise to the self-assembly of linear polymeric, random surface ("membrane"), tubular ("nanotube"), and hollow icosahedral structures that are similar in many respects to their biological counterparts. The potentials involve *equivalent particles* and an interplay between directional (dipolar, multipolar) and short-range (van der Waals) interactions. Specifically, we find that the dipolar potential, having a continuous rotational symmetry about the dipolar axis, gives rise to chain formation, while particles with multipolar potentials, having discrete rotational symmetries (square quadrupole or triangular ring of dipoles or "hexapole"), lead to the self-assembly of open sheet, nanotube, and hollow icosahedral geometries. These changes in the geometry of self-assembly are accompanied by significant changes in the kinetics of the organization.

DOI: 10.1103/PhysRevE.73.031502 PACS number(s): 61.20.Qg, 87.16.Ka, 81.16.Dn, 87.16.Dg

I. INTRODUCTION

Molecular self-assembly at equilibrium is central to the formation of numerous biological structures [1–3], and the emulation of this process through the creation of synthetic counterparts [4–9] offers great promise for nanofabrication [10–15]. The central problems in this field are an understanding of how the symmetry of interacting particles encodes information about the geometry of the organized structure and the nature of the thermodynamic transitions governing this type of self-organization process. Our approach is inspired by a long tradition of modeling and precise experimental observations on the self-assembly of biological structures: chainlike polymers (actin [16–19] and crystallin proteins [20]), fiberlike polymers (tobacco mosaic virus [21–23], sickle cell hemoglobin [24–27], type-1 collagen [28] and amyloid fibers), hollow cylindrical structures such as membrane ion channels [29–32] and tubulin [33–38], and the normally icosahedral shell structures of "spherical" viruses ("capsids") [39–47] and of clathrin-coated vesicles involved in endocytosis [48].

The term "self-assembly," and indeed a whole field of scientific inquiry, was initiated by the remarkable observation that the sheath proteins and RNA components comprising tobacco mosaic virus could spontaneously regenerate themselves into active viruses *in vitro* [21,22]. Moreover, it was also found that the rodlike protein sheath could regenerate itself even without genetic material (RNA) in its core. These seminal observations prompted further investigations into the nature of this highly specific, but apparently equilibrium-based, organizational process. Self-assembly of spherical viruses under *in vitro* conditions was later observed in the nearly spherical cowpea chlorotic mottle virus. [22] These developments were greatly facilitated by advances in electron microscopy and x-ray diffraction that have enabled the resolution of virus molecular structure with atomic-scale resolution [1]. Further measurements indicated that while other viruses had the rodlike form of tobacco mosaic virus, spherical viruses were actually more common and were prevalent in both plant and animal viruses. This naturally led to speculations into the physical origins into this regularity of viral form and to the first theoretical modeling of biological self-assembly [3,39].

It is now known that many viruses contain only enough genetic material for replicating a few proteins, and it has been appreciated experimentally since the pioneering work of Rosalind Franklin [23] that the organization of viral protein sheaths must involve particles having *equivalent* or nearly equivalent molecular structure. Crick and Watson hypothesized that the assembly of such equivalent particles could only occur by the formation of highly symmetric shell structures [39]. In particular, they suggested that the shells should take the form of tubes (helical in general) or closed structures belonging to a family of regular polyhedra (i.e., Platonic solids: cube, tetradedron, octahedron, dodecahedron, icosahedron) where each particle has a local environment that is *equivalent* to its neighbors. These arguments amount to a suggestion that the local potentials of the particles within these shells are *invariant under particle permutation* P. Crick and Watson's ideas [39] were subsequently supported by electron microscopy and x-ray diffraction measurements for polio and later other spherical viruses were found to form structures having icosahedral symmetry [1,40,44].

While the icosahedral shell is a natural structure for encapsulating genetic material within the family of Platonic solids, given its relatively large volume-to-surface area ratio, it was also found that other icosahedral symmetry viruses violated the strict *equivalence principle* [39]. Evidently, a

*Electronic address: vanw@usna.edu
†Electronic address: jack.douglas@nist.gov

strict equivalence of local molecular environments within a capsid severely limits the size of these structures and it was later found that spherical viruses overcome this constraint by utilizing structures built up from subcomponents having both fivefold and sixfold local rotational symmetries. Caspar and Klug [3], with input from architectural theorist Buckminster Fuller and his students, interpreted this "molecular differentiation" process in virus shell organization through a generalization of the arguments of Crick and Watson. In their classic paper on virus structure [3], they replaced the constraint of perfect equivalence by the hypothesis of "quasiequivalence," which requires that the defect energy associated with inequivalent molecular environments to be minimized. For the closed-shell spherical viruses, this *principle of quasiequivalence* implies that spherical viruses must comprise a *unique* family of icosahedral symmetry surfaces ("icosadeltahedra") having local fivefold and sixfold symmetries [1,3]. In particular, a perfect icosahedron of 60 equivalent proteins has 20 faces, while the larger icosadeltahedra contain, in general, an integer-T multiple of 60 capsid proteins where the factor T is termed the "triangulation factor." There are two topological indices (h and k) that determine how the hexagons are placed in these structures and that determine the allowable quantized T values ($T=k^2+hk+h^2$ where h and k are non-negative integers such that $T \geqslant 1$) [3]. Remarkably, these quasiequivalent structures describe all but a small number of spherical viruses [1,3]. The principle of quasiequivalence in the biological community is currently considered to be fundamental to understanding virus structure and, more broadly, biological self-assembly.

Unfortunately, the formal symmetry-based arguments of Crick and Watson [39] and Caspar and Klug [3] do not provide any insight into the thermodynamic factors governing this sort of self-assembly; nor do they provide any specific indication of what the term "quasiequivalent" really means in terms of molecular potentials and the proteins actually involved in this type of assembly process. In particular, there is the question of why the capsid proteins would assemble into a hollow shell in the first place. These questions are practically important because the development of strategies for treating viral diseases through interrupting this self-assembly process requires an understanding of the kinetics of viral capsid self-assembly, as well as an understanding of the thermodynamic parameters governing the capsid stability [45]. These concerns have natually led to attempts to simulate virus self-assembly and structure.

Bruinsma and co-workers [46,47] recently offered a physical explanation of quasiequivalence in terms of molecular conformational transitions ("molecular switches") of the capsid protein molecules, an explanation often advocated heuristically by biologists [3]. In particular, they concluded that multiple particle "internal states" must be involved for the quasiequivalent structures of Caspar and Klug to arise as low-energy equilibrium structures. Notably, the modeling of Bruinsma and co-workers does not actually address the self-assembly process itself, but rather the relative energies of fully assembled viral capsid structures. (This model will be discussed in further detail below where we show that protein molecular switches are *not required* to generate quasiequivalent structures in our multipole interaction model fluids.)

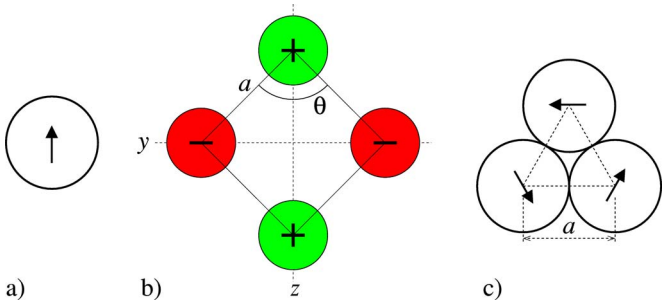

FIG. 1. (Color online) Schematic representation of a dipole, quadrupole, and hexapole interactions. (a) Dipole. (b) "Square" quadrupole indicated by $\theta=\pi/2$. A "linear" quadrupole corresponds to the limit $\theta=0$. (c) Hexapole formed by three dipoles at the vertices of a triangle with a head-to-tail orientation where $a=\sqrt{3}$.

There has also been interesting recent work addressing the self-assembly process itself based on equilibrium polymerization models of the formation of icosahedral shells [45]. This approach is apparently able to describe important aspects of the virus self-assembly thermodynamics and kinetics, but this kind of coarse-grained kinetic assembly model does not provide much insight into what aspects of the protein interaction potentials actually give rise to icosahedral shell organization. We also note pioneering molecular dynamics investigations of the self-assembly of icosahedral structures by Rapaport and co-workers [49], which uses "prefabricated" equivalent subunits and achieves their assembly into icosahedral shell structure by adjusting their interactions and temperature. This work provides a specific example of self-assembly into closed-symmetric-shell structures from equivalent particles that seem to follow the equivalence principle of Crick and Watson [39]. However, these simulations do not lead to the self-assembly of hexagonal and pentagonal subunits that are prevalent in measurements on viral assembly, so the simulations must still be regarded as rather rudimentary models of viral capsids. We find a coexistence of hexagonal and pentagonal subunits in our simulations below, along with the self-assembly of icosahedral shells, providing some further insights into how such structures might form and the origin of quasiequivalence and polymorphic assembly more generally.

Stimulated by the philosophical approaches of Crick and Watson [40] and Caspar and Klug [3] and recent attempts to simulate viral self-assembly and structure [46,68], we introduce a family of minimal models that can serve as a testing ground for understanding principles of self-assembly. Our approach builds on our systematic investigation of the Stockmayer fluid (SF), which is an ideally simple model of particle self-assembly that incorporates the basic competition between directional (dipolar) and isotropic (van der Waals) interactions [see Fig. 1(a)], which is apparently key to many real self-assembling systems [50–52]. The SF is a natural starting point for investigating protein assembly since proteins are often characterized by extremely large dipolar interactions [e.g., the dipole moments of tubulin, collagen, and hemoglobin(S) are 1410 D, 1150 D, and 545 D, respectively [53] where 1 Debye (D) $=3.336\times10^{-30}$ C m] or directional hydrogen bonding interactions, and it is rather likely that these highly directional interactions are relevant to any

physical explanation of protein viral capsid self-assembly. Numerous previous experimental studies of *in vitro* viral self-assembly have shown that electrostatic interactions are implicated in the self-assembly process [54]. Moreover, recent simulations of charged-particle fluids [55] indicate a strong propensity for the charged species to organize in *multipole clusters*, so it is natural to consider multipole potentials in developing generalizations of the SF potential that have different symmetry characteristics. In particular, below we consider a quadrupolar generalization of the SF that models two head-to-tail dipoles or four charged particles (two plus and two minus charged particles) in a ring [see Fig. 1(b)] and a triangular configuration of SF particles at the vertices of a triangle in a head-to-tail orientation [see Fig. 1(c)]. Such triangular configurations of proteins have been directly observed in proteins forming viral capsids, and this model is further motivated below [56].

While the symmetry arguments of Crick and Watson [16] do not make predictions for the form of self-assembly (e.g., tetrahedron versus icosahedron) in relation to the symmetry properties of the organizing particles, we may formally extend their reasoning by hypothesizing that the local rotational symmetries governing the directional interactions of the self-assembling particles tend to be *locally preserved* in the self-assembled structure. We see that the dipolar potential in Fig. 1(a) has a $C_{\infty v}$ point-group symmetry and thus has a continuous rotational symmetry. The square quadrupole ($\theta=\pi/2$) generalization of the SF [52] in Fig. 1(b) exhibits a discrete (D_{2h}) point-group symmetry, while the triangular configuration of SF particles in Fig. 1(c) has a discrete C_3 rotational symmetry normal to the plane containing the dipoles. Our requirement that these potentials preserve their local symmetries in the organized structure requires the formation of *linear polymeric structures* in the case of the SF, while *two-dimensional polymers* are predicted for discrete rotational potential generalizations of the SF. In particular, we expect that the potentials in Figs. 1(b) and 1(c) to give rise to irregular two-dimensional polymers ("random surfaces") having local rectangular and hexagonal structures, respectively. We emphasize that it is primarily the *symmetries* of the directional interactions in these potentials that are important for our considerations below and similar particle assemblies to those found for the multipole potentials can be expected for other particle interaction potentials (hydrogen bonding, π-π interactions and localized hydrophobic interactions, strong-segregation block copolymers in solution, grafted polymer chains on nanoparticles having attachment points of prescribed symmetry, etc.) sharing the same point-group symmetries as the multipole potentials that we considered. Zhang and Glotzer [57] have recently considered other interesting examples of self-assembly with local short-range directional interactions that illustrate this point.

Our simulations validate our symmetry arguments relating the symmetry characteristics of the particles to those of the self-assembled structures. Specifically, a dipolar potential, having a continuous rotational symmetry about the symmetry axis, leads to chain formation at equilibrium [50] (equilibrium polymerization [58]), while changing to a potential having twofold and threefold discrete rotational symmetries (e.g., square quadrupole interaction or triangular ring of dipoles, respectively) leads to the self-assembly of random surfaces and to nanotube and icosahedral shell structures resembling those found in the self-assembly of tubular or icosahedral viruses [1,3,41–47]. (The closing of two-dimensional polymers in one and two coordinate directions to form nanotubes and icosahedral shells is the analog of ring formation for two-dimensional polymers.) We also find that these changes in assembly organization with the symmetry of the interaction potential are accompanied by *qualitative* changes in the character of the thermodynamic assembly transition that were not initially anticipated. We devote much of our attention below to characterizing these changes in the self-assembly dynamics.

The multifunctional nature of the associations for the particles with mutipolar interaction leads to strong fluctuations in the time at which self-assembly initiates and other features that resemble ordering in supercooled liquids where a first-order phase transition is involved. Curiously, this behavior simply does not exist for particles whose directional interactions involve a continuous rotational symmetry (e.g., the SF). We find that this change in the nature of the self-assembly transition in the formation of two-dimensional polymers allows for the selective formation of distinct morphologies under the same thermodynamic conditions through a control of the "seed" geometry and interaction potential. We also find that directional growth along a particular direction ("polar growth"), as found in certain biological systems (e.g., tubulin and its structural analog in plants) [35–37], can be induced by controlling the symmetry properties of the seed. These properties (a strong sensitivity of organization to rare "nucleation" events, fibrous, directional growth, etc.) are characteristic of molecular self-assembly in many important biological systems, including sickle cell disease [24–27] and neurodegenerative diseases (Alzheimer's, Down's syndrome, etc.) [30–32]. Self-assembly processes of this kind are also relevant to a wide range of commercial additive materials called "gelators" that self-organize into nanoscale fiber structures [59–69] and to synthetic peptide gels promising for tissue engineering applications [70–72].

II. MULTIPOLE INTERACTION MODELS AS MINIMAL MODELS OF SELF-ASSEMBLY

A. Stockmayer fluid

First, we briefly recall some basic aspects of self-assembly in the Stockmayer fluid [50]. Specifically, two SF particles interact via a Lennard-Jones (LJ) potential and an additional point-dipole potential placed at the center of each particle [Fig. 1(a)]. The dipolar contribution to the interaction potential is given by

$$u_{\text{dipole}} = (\boldsymbol{\mu}_i \cdot \boldsymbol{\mu}_j)/\mathbf{r}_{ij}^{\,3} - 3(\boldsymbol{\mu}_i \cdot \mathbf{r}_{ij})(\boldsymbol{\mu}_j \cdot \mathbf{r}_{ij})/\mathbf{r}_{ij}^{\,5}, \qquad (1)$$

where μ_i is the dipole moment of particle i and $\mathbf{r}_{ij}=\mathbf{r}_i-\mathbf{r}_j$ is the interparticle separation, and the LJ contribution to the potential ($u_{SF} \equiv u_{LJ}+u_{\text{dipole}}$) equals

$$u_{LJ} = 4\varepsilon[(\sigma/\mathbf{r}_{ij})^{12} - (\sigma/\mathbf{r}_{ij})^{6}], \qquad (2)$$

where the van der Waals (vdW) interaction energy ε is a measure of the "strength" of the vdW interaction and σ char-

acterizes the particle "size." It is conventional to define a dimensionless measure of the dipolar interaction energy relative to the vdW energy, $(\mu^*)^2=\mu^2/\varepsilon_D\sigma^3\varepsilon$ where ε_D is the dielectric constant of the medium to describe the relative strengths the directional to the isotropic interactions in the SF. Physically, the dipolar interaction energy $\mu^2/\varepsilon_D\sigma^3$ equals the Coulombic interaction energy between two charged hard spheres of common diameter σ and valence that are in contact, where μ equals the charge magnitude q times the charge separation σ—i.e., $\mu=|q|\sigma$. For all the simulations below involving SF particles, we take $\mu^*=6$, unless otherwise stated. With this choice of dipole strength, the dipolar contribution to the minimum in the potential is roughly 100 times the LJ contribution (see below) so that the directional interaction predominates [50–52]. All densities ρ reported in this paper are number densities, and T is normalized by the vdW energy ε/k_B, where k_B is Boltzmann's constant. We have discussed self-assembly in the SF model in detail in a previous paper [50], and in the present work we confine ourselves to the properties of this model that have relevance to our discussion of the multipole models that generalize the SF.

B. Quadrupole-vdW fluid

The inclusion of a quadrupole interaction [Fig. 1(b)] superimposed on the van der Waals interaction is a direct formal generalization of the SF [73–75]. The LJ component of the potential is the same as in Eq. (2). The *point-quadrupole* interaction between two *linear* quadrupoles [$\theta=0$ in Fig. 1(b)] of magnitude Q_i and Q_j whose orientations are described by the unit vectors $\bar{e}_i$ and $\bar{e}_j$ can be written as

$$u_{ij}=\frac{3}{4}\frac{Q_iQ_j}{r_{ij}^5}[1-5\cos^2\theta_i-5\cos^2\theta_j-15\cos^2\theta_i\cos^2\theta_j+2(\cos\gamma_{ij}-5\cos\theta_i\cos\theta_j)^2],$$

$$\cos\theta_i=\frac{\bar{e}_i\cdot\overline{r_{ij}}}{r_{ij}},\quad \cos\theta_j=\frac{\bar{e}_j\cdot\overline{r_{ij}}}{r_{ij}},\quad \cos\gamma_{ij}=\bar{e}_i\cdot\bar{e}_j. \tag{3}$$

More generally, the energy between two pure quadrupoles i and j is given by [73]

$$u_{ij}=\frac{1}{9}\bar{\bar{Q}}_i:\bar{\bar{\bar{T}}}_{ij}:\bar{\bar{Q}}_j, \tag{4}$$

where

$$\bar{\bar{\bar{T}}}_{ij}=\bar{\nabla}\bar{\nabla}\bar{\nabla}\bar{\nabla}\frac{1}{r_{ij}},\quad r_{ij}=(\bar{r}_{ij}\cdot\bar{r}_{ij})^{1/2},\quad \bar{r}_{ij}=\bar{r}_i-\bar{r}_j.$$

A pure quadrupole charge configuration is defined to have a zero net charge (i.e., monopole strength is zero) and the dipole and higher multipole interactions (octapole and higher-order multipoles) are also taken to be zero. An example of such an ideal quadrupole configuration of *discrete charges* is shown in Fig. 1(b). The quadrupole moment tensor for a molecule i consisting of N_i discrete (point) charges of charge q_j is given by,

$$\bar{\bar{Q}}_i=\sum_{j=1}^{N_i}q_j(3\bar{r}_j\bar{r}_j-r_j^2\bar{\bar{\delta}}). \tag{5}$$

More specifically, for the four-particle configuration shown in Fig. 1(b), consisting of four point charges of common charge magnitude q and charge separation a between plus and minus charges, the quadrupole moment tensor reduces to the matrix representation

$$\bar{\bar{Q}}=4a^2q\begin{bmatrix}-\frac{\cos\theta}{2} & 0 & 0\\ 0 & \frac{\cos\theta-3}{4} & 0\\ 0 & 0 & \frac{\cos\theta+3}{4}\end{bmatrix}. \tag{6}$$

This represents the quadrupole moment tensor for a pure quadrupole in its principle axis frame where the matrix becomes diagonal. The limit $\theta\to 0$ recovers the case of a linear quadrupole oriented along the z axis where we have

$$\bar{\bar{Q}}_{\text{linear}}=4a^2q\begin{pmatrix}-1/2 & 0 & 0\\ 0 & -1/2 & 0\\ 0 & 0 & 1\end{pmatrix}. \tag{7}$$

Given that Eqs. (3) and (4) for $\theta=0$ are equivalent if $Q=4a^2q$, we write the quadrupole moment tensor for a pure quadrupole in its principle frame as

$$\bar{\bar{Q}}=Q\begin{bmatrix}-\frac{\cos\theta}{2} & 0 & 0\\ 0 & \frac{\cos\theta-3}{4} & 0\\ 0 & 0 & \frac{\cos\theta+3}{4}\end{bmatrix}, \tag{8}$$

where $Q=4a^2q$ is taken to be a general "strength parameter" of the quadrupole interaction. However, the interaction energy between two pure quadrupoles also depends on the "quadrupole angle parameter" θ so that two parameters are required to specify this potential. Similar to the SF, we define a reduced quadrupole interaction strength relative to the van der Waals interaction as $Q^*=Q/(\varepsilon_D\sigma^5\varepsilon)^{1/2}$. The reader is warned that there are multiple definitions of the quadrupole interaction strength in the literature that differ by constants of proportionality [73–75].

Surprisingly, previous simulations with the quad-vdW fluid have generally been restricted to the "linear quadrupole," corresponding to $\theta=0$ in Eq. (6) [see Fig. 1(b)]. For example, the critical properties of fluids with linear quadrupole interactions are investigated in Refs. [73–75] Dijkstra and co-workers describe clustering in exfoliated clay solutions [76] in terms of a linear quadrupole interaction and found the formation of branched equilibrium polymer structures rather than the linear chains found for the SF, a result that is echoed in our results below where we briefly consider the case ($\theta\neq\pi/2$). The square quadrupole potential ($\theta=\pi/2$) indicated Fig. 1(b) is characterized by having a two-

fold rotational symmetry about the plane containing the charges in the discrete particle cluster analog of this potential. Below we find that this property gives rise to a general tendency to the formation of sheetlike polymers with a rectangular local symmetry, as suggested in the Introduction.

C. Hexapole fluid with van der Waals interaction

It is evident that many self-assembling structures do not have the local rectangular symmetry exhibited by the quad-vdW fluid model and otherwise do not form one-dimensional polymeric structures as in the SF fluid. Many structures exhibit threefold, fivefold, or even higher-order *discrete rotational symmetries*. A threefold symmetry is evident, for example, in the faces of icosahedral viral capsids [1] and the hexagonal lattice structure of certain tubular virus structures [77]. We next introduce a schematic model of the multipole class that provides some insights into growth forms having these other symmetries.

A threefold local rotational symmetry can be generated by simply placing SF particles at the vertices of triangles in a head-to-tail configuration [Fig. 1(c)] to obtain a "hexapole" or "triangular dipole" potential, augmented by van der Waals interactions (hex-vdW model). For simplicity, the dipole strength, van der Waals radius, and other parameters are taken to be exactly the same as in SF [Fig. 1(a)]. As mentioned earlier, triangular configurations of proteins have been directly observed in the structures of capsid proteins [56] so that this structure is plausible for modeling virus assembly.

It should be appreciated that the triangular structures of the hexapole model do not naturally arise in the SF since there is a relatively large bending rigidity induced by the dipole interaction that inhibits small ring formation when the dipole strength is large [50]. However, such triangular assemblies probably form if the monomers had a anisotropic shape such that they fit together into a triangular shape with strong hydrophobic interactions at their boundaries to link the dipolar elements. Such "pre-assembly" is known to occur in the formation of clathrin cages where the three clathrin proteins molecules form trimer structures by joining at one of their ends to a common hub through the formation of a charge complex [48,49]. These "triskelion" (self-assembled three-arm star polymer) structures are the basic assembling unit of clathrin cages [48,49] and were the inspiration for our hexapole model. In general, it should be possible to form modular structures having a variety of point group symmetries by the "tiling assembly" mechanism proposed for viral "capsomers" or by the local chain association mechanism of triskelions. By varying the particle interactions it should also be possible to have the subunits form "protomers" such that the capsomeres and triskelions have distinct self-assembly transitions from the organization of the structures into a larger-scale superstructure. Increasingly complex structures could be "programmed" in this fashion.

D. Monte Carlo simulation methods

The simulation of strongly associating systems can present serious computational challenges. The strong binding energies between associated particles and large distances between nonassociated particles can make sampling of important regions of configuration space difficult [78]. The time required for particles to undergo an association-disassociation transition can be very long compared to typical molecular dynamics simulation times. There are Monte Carlo algorithms that can overcome these difficulties, however. Here we use the aggregate bias Monte Carlo algorithm [79] to improve the sampling of relevant regions of configuration space and enhance the formation of clusters. At the heart of this algorithm is an intrabox swap move that is targeted at sampling the formation or destruction of clusters. We also implement the simple translational and rotational moves to explore nearby regions of phase space. A discussion of this method is given in our previous paper devoted to the SF [50].

The interaction between particle pairs was truncated at half the box length. This boundary condition was motivated by previous results for the SF that indicated the treatment of the full long-range potential using Ewald summations was not necessary for the density and T range considered here [50]. We have also chosen the range of T, densities, and interaction strengths to avoid complications from phase separation as much as possible. The densities are in the range 0.001–0.02. While the critical points of these fluids are not known, we did not observe any evidence of phase separation (coexisting phases) for the conditions we investigated. The determination of critical temperature and compositions of these fluids would be a necessary step for studying these fluids at higher densities.

III. RESULTS

A. Stockmayer fluid

In a previous investigation [50], we studied the SF as a model of self-assembly and mapped out the thermodynamic transition lines for this fluid as a function of ρ and T. We briefly review some of the relevant properties of this model, before extending our discussion to our new results for the quad-vdW and hex-vdW fluids.

The dipolar interaction leads to a strong propensity for the dipolar particles to associate in a head-to-tail configuration and upon cooling the particles polymerize into long polymer chains that form and disintegrate in dynamic equilibrium (see Fig. 2) [50]. We see from Fig. 2 that the continuous rotational symmetry about the dipolar axis is nearly preserved in the polymer chains that form in these fluids and these angular degrees of freedom lead to the formation of particle chains having roughly random walk configurations. This figure shows some representative particle configurations above ($T=10.0$) and below ($T=7.80$) the polymerization transition temperature $T_\Phi=9.5$ for a particle concentration $\rho=0.001$. The transition temperature T_Φ separating the dissociated and self-assembled thermodynamic states (not thermodynamic phases, however) is defined by an inflection point in the T dependence of the *extent of polymerization*, Φ (fraction of particles in the "polymerized" state) [50,58]. In previous work [50], we found that the theory of equilibrium polymerization [58] describes this equilibrium polymerization transition rather well, where the interparticle association

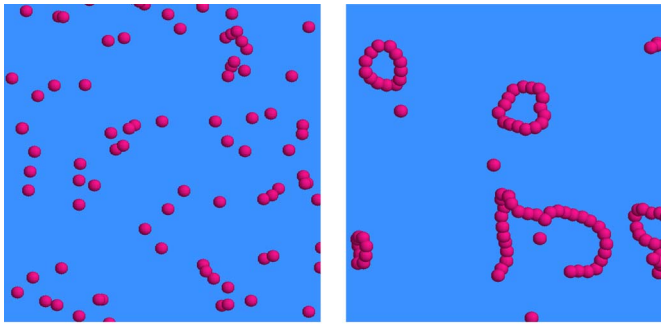

FIG. 2. (Color online) Representative configurations of the Stockmayer fluid above and below the polymerization temperature T_Φ. (a) $T=10$, (b) $T=7.80$. The density is constant, $\rho=0.001$ and $T_\Phi=9.5$. In Ref. [50], we reduced T by the critical temperature of the LJ fluid ($T_c \approx 1.3\varepsilon$) rather than the strength of the vdW interaction ε so that the reported temperatures have smaller magnitude.

("sticking") energy was uniquely fixed by the magnitude of the energy minimum in the intermolecular potential between two SF particles [50]. At low temperatures, the long-range dipolar interaction causes the chains to form ring structures that minimize the field energy of the polymeric structures, but the analytic modeling has not been developed to fully account for these topological effects on the nature of particle assembly [50,80–82]. Recent work indicates that the low-energy polymer configurations exhibit nontrivial knot configurations when the van der Waals and dipolar energies in the SF have comparable magnitudes [81], so these topological aspects of the assembly process have clear relevance for understanding self-assembly in real systems. Many basic questions remain about how the topology and disordered geometry of the assemblies affect the interactions and organization of these objects into larger-scale assemblies and the SF provides an interesting model system for exploring these questions in the future.

Below we consider the scaling relation between the cluster radius of gyration, R_g, and the cluster mass that defines the fractal dimension of clusters and which provides a distinguishing characteristic in scattering studies of self-assembling systems. We recall here that the radius of gyration of the SF chains exhibits a nontrivial scaling with mass, $R_g \sim M^\nu$, where $\nu \approx 0.68$ [50]. In the next section, we consider the counterpart of this relation for particles with a square quadrupole interaction where random surface polymers form instead of linear polymers.

Our previous paper did not consider the *dynamics* of self-assembly, and we briefly summarize aspects of the assembly kinetics in the SF that are relevant to our discussion below. Figure 3 shows the growth of the extent of polymerization $\Phi(t)$ to its asymptotic long-time value Φ for T near ($T=11.1$) and below ($T=7.86$) the polymerization transition temperature [50] $T_\Phi=11.3$ for $\rho=0.04$. We observe that the rate of self-assembly $[d\Phi(t)/dt]$ increases with the magnitude of the "quench depth," $\tau_\Phi=|T-T_\Phi|/T_\Phi$, and that the amplitude of the fluctuations progressively diminishes with increasing τ_Φ. In the experimental literature, curves which monitor the extent of polymerization $\Phi(t)$ in time are conventionally termed "progress curves" [25]. The long-time

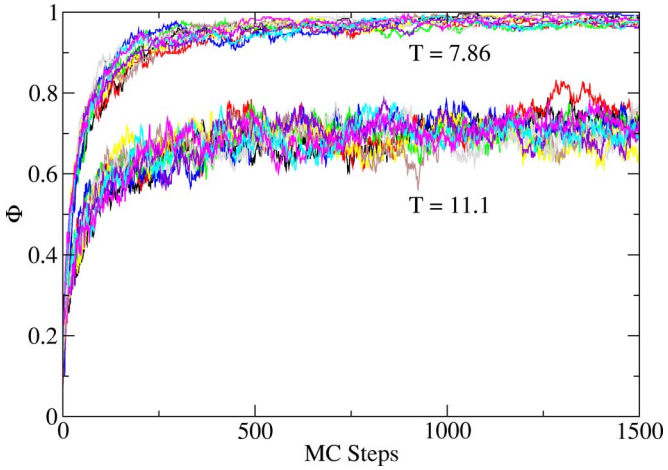

FIG. 3. (Color online) Progress curves $\Phi(t)$ for Stockmayer fluid at low and moderate quench depths. Upper curve indicates $\Phi(t)$ for a relatively deep quench ($T=7.86$), while the lower curve indicates $\Phi(t)$ near the polymerization transition, $T=11.1$. The density is constant, $\rho=0.04$ and $T_\Phi=11.3$.

limit of $\Phi(t)$ determines the equilibrium value $\Phi(t\to\infty)$ of the polymerization "order parameter," and only such equilibrium quantities were reported in our previous paper [50]. Fluctuations are evident in Fig. 3 as chains associate and dissociate in *dynamic equilibrium*, the amplitude of the fluctuations in $\Phi(t)$ and other thermodynamic properties (average energy E, chain length L, etc.) becoming larger and increasingly long lived near T_Φ. This explains the maximum in the specific heat C_p that occurs near T_Φ, which is a characteristic observable feature in experimental or computational studies of self-assembling systems.

We see from Fig. 3 that raising T within the polymerized regime leads to a *smooth decrease* in the average chain length L as the system reverts to monomers for $T \gg T_\Phi$. The chain growth upon cooling and shrinkage upon heating are quite reversible, and no nucleation seems to be required for these processes to occur. This mode of growth, which seems to be observed in the equilibrium polymerization of actin [17], is strikingly different from our findings for the quad-vdW and hex-vdW fluids below where *two-dimensional* polymer morphologies form rather than linear chains and where large fluctuations in the time at which growth initiates occurs.

While the interpretation of Monte Carlo (MC) generated dynamics as a real molecular dynamics is not strictly correct from a physical standpoint, it should provide a reasonable qualitative description of the organizational dynamics. For example, a monotone increase in Φ and increasingly rapid rate of polymerization occur with increasing quench depth in actin polymerization (actin polymerizes upon heating so that we define quench depth generally as the absolute value of temperature difference between the T at which polymerization occurs and T_Φ) and in the dynamics of many other self-assembling systems. Previous work has established the validity of MC simulations in reproducing essential characteristics of the dynamics of associating polymers [83,84].

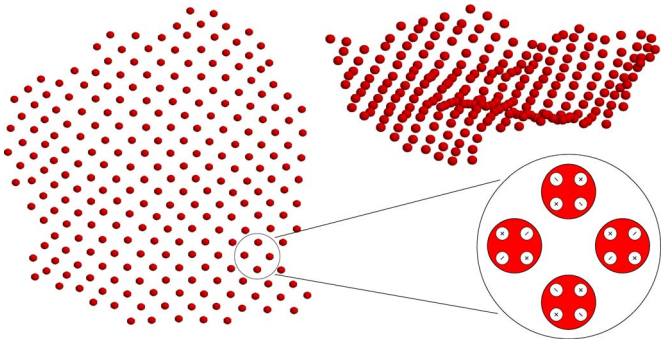

FIG. 4. (Color online) A sheet formed by square quadrpole–van der Waals fluid. The figure to the left indicates a view of a representative two-dimensional random surface formed at low T from the top, and the top right image shows a profile view. The "charge orientation" within the quadrupoles is indicated at the bottom right. System conditions: $T=1.35$, $Q^*=1.0$, and $\rho=0.001$.

B. Quadrupole/vdW fluid

Although the local symmetry associated with the ability of SF particles to freely rotate and translate in space is broken when linear polymer chains begin to form upon cooling, the freedom of these the particles to rotate about the local chain axis between the particles remains preserved in the organized structure. This rotational freedom causes the resulting structures to be "floppy" and one-dimensional in nature. The *discrete rotational symmetry* of the quad-vdW fluid [Fig. 1(b)] gives rise to extended polymer structures that preserve the discrete local rotational symmetry within the organized structure. In Fig. 4, we show a representative "random surface" polymer that spontaneously organizes in the quad-vdW fluid at low temperatures ($T=1.35$). These structures are evidently invariant under local twofold rotations within the random surface so that this symmetry of the individual particles is indeed preserved in the organized structure. We also find that the "dipoles" comprising the quadrupole have a strong tendency to form closed loops as in the SF. The reason is the same, minimization of the energy of the resulting cluster [50,80–82]. Thus, the organizations of the SF and quad-vdW fluids are both driven by directional interactions and the preservation of local symmetries in the single-particle potential. The polymerization process also leads to structures with nontrivial topological structures depending on the system conditions. These structures are expected to be especially complicated when the quadrupole interaction has a comparable magnitude to the van der Waals interaction, as in the SF model, under conditions for which the magnitude of the dipolar and van der Waal interactions are comparable [81].

The self-interactions of these assembling surfaces involve both excluded-volume and long-range quadrupolar interactions, so it is not clear whether the geometry of these random surfaces should be the same as self-avoiding surfaces or even whether a universal scaling should exist at all. We briefly address this important aspect of random surface formation in this model in Fig. 5 where we show the scaling of R_g of these two-dimensional polymers against the number of particles, N, in the clusters. The data are for a range of quench depths ($T=1.35-2.0$, $\rho=0.001$, $Q^*=1.0$) and lead to a remarkably robust apparent scaling exponent describing these random

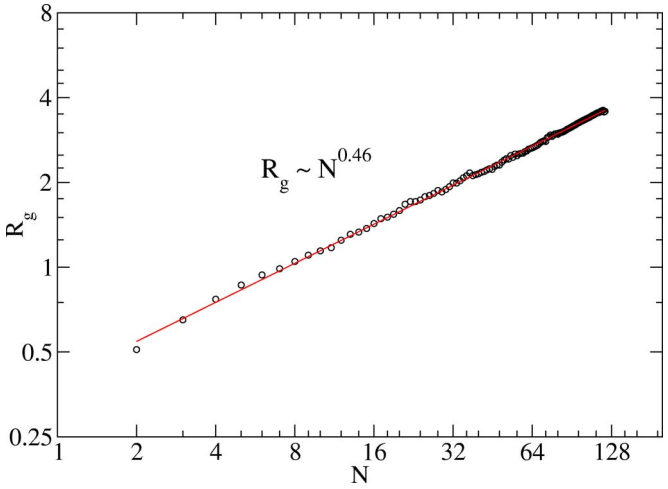

FIG. 5. (Color online) Random sheet radius of gyration, R_g vs mass N. System conditions: $Q^*=1.0$, $T=1.35-2.0$, and $\rho=0.001$.

surfaces, $R_g \sim N^{0.46\pm0.02}$. (The uncertainty is estimated by determining the range of exponent values that are consistent with fitting the data over the range $10 \leqslant N \leqslant 100$ rather than as an estimate of systematic error.) The scaling exponent $\nu=0.46$ is somewhat smaller than the exponent $\frac{1}{2}$ expected for ideal self-avoiding surfaces in three dimensions [85(a)], so that these random surfaces seem to be somewhat more "crumpled," rather than simple flat self-avoiding surfaces where $\nu=\frac{1}{2}$ in three dimensions [85(a)]. Some crumpling is visually apparent in the spectrin protein network that provides the scaffold for red blood cell membranes where an exponent ν near 0.42 has been reported from scattering measurements [86].

We can appreciate how the rectangular local symmetry of these random surfaces is encoded by the square quadrupolar potential by examining the impact of modifying the angle θ defining the "asymmetry" of the quadrupolar potential [see Fig. 1(b)]. Changing θ from $\pi/2$ to $\pi/4$, an angle intermediate between the square and linear quadrupole, *destroys* the local square rotational symmetry evident in Fig. 4, and Fig. 6 illustrates how this symmetry breaking impacts the self-

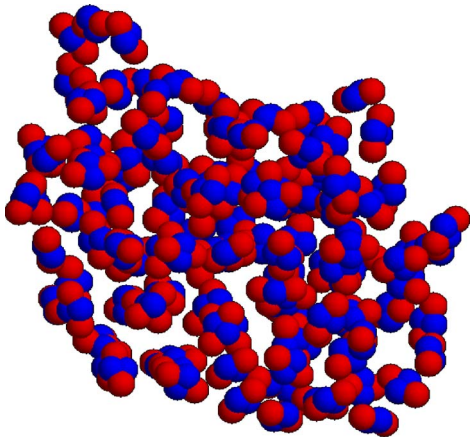

FIG. 6. (Color online) Self-assembly in the quad-vdW fluid with intermediate angle $\theta=\pi/4$. The angular constraint creates packing frustration, leading to a more disordered polymeric structure. System conditions: $Q^*=2.0$, $T=1.9$, and $\rho=0.02$.

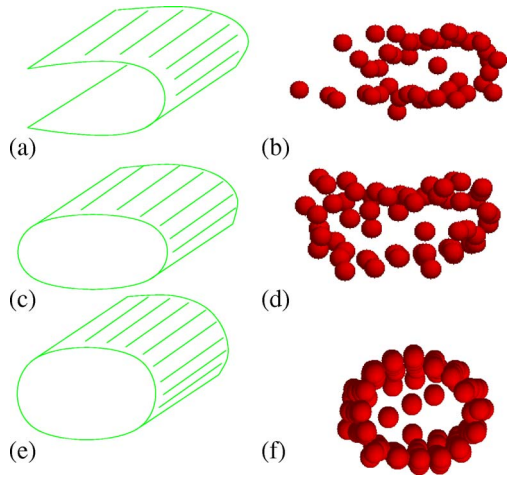

FIG. 7. (Color online) Formation of a nanotube in the quad-vdW fluid. The tube forms through the formation of a two-layer structure, and seams then form at the edge. This process is schematically indicated in (a), (c), and (e) and corresponding particle configurational realizations are shown in (b), (d), and (f). Once the edges form, the layers open up to form a nanotube. This evolution can occur by sheet folding, but more often arises from the formation of bilayer sheets. System conditions: $T=1.7$, $Q^*=2.0$, and $\rho=0.001$.

assembly morphology. Apparently, if the generalized quadrupole particles cannot "find" a well-defined surface tiling geometry, then they, by default, organize into branched polymer structures instead. Previous simulations for *linear quadrupole* particles with an additional frustrating anisotropic hard-core interaction superimposed to model the anisotropic shape of the clay particles likewise led to the formation of branched equilibrium polymers [76]. Despite the disordered appearance of the branched polymers in relation to their random surface counterparts, it has been shown that branched polymer and random surfaces with excluded-volume interactions share common scaling characteristics so that branched polymers can be considered from a topological standpoint as being perforated random surfaces as far as their universality characteristics are concerned [85(a)]. We thus expect the R_g of these branched polymer structures to be the *same* as for the random surfaces shown in Fig. 4. These and many other aspects of the geometry of self-assembled structures in the quad-vdW model require further study. Our main point here is that they exhibit well-defined geometrical statistical properties that are potentially universal for this class of potentials.

We have previously indicated a general tendency for SF particles to form ring polymers at low T [50], and we now show that this phenomenon has its counterpart in the quad-vdW fluid. Figure 7 shows that the sheet polymers of the quad-vdW model tend to form tubes. The process by which these nanaotubes form in our model calculations is curious. The first stage of this process [Figs. 7(a) and 7(b)] involves the formation of a bilayer sheet (a structure that we refer to as "pita bread" since this layer structure is susceptible to opening and to particles entering this cavity). The particles within these bilayer sheets stagger within adjacent layers, and this leads to the formation of moiré patterns in the stacked layers [Fig. 8(a)]. (Such "checkerboard" patterns

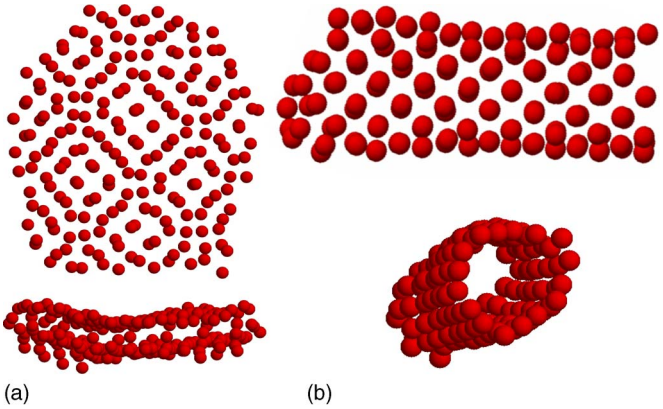

FIG. 8. (Color online) Self-assembly of nanotubes in the quad-vdW fluid. (a) Left top images are top and side views of a two-layer ("pita") structure formed in the square quad-vdW fluid. (b) Top right and bottom right images are side and profile views of the tube shown in Fig. 6(f). System conditions: $Q^*=2.0$, $T=1.4$, and $\rho=0.02$. (b). System conditions: $T=1.7$, $Q^*=2.0$, and $\rho=0.001$.

have been observed in tubular structures formed by the polyoma virus [42].) These bilayer sheets form either through sheet folding or more commonly through an initial stacking into multilayer sheets. There is a natural tendency for these layers to close off at their edges and for the layers to open up afterwards, apparently to reduce the energetic cost of these bare edges [Figs. 7(c) and 7(d)]. It is through this rather involved process that the nanotubes "initiate" or "nucleate" in our simulations. (The term "nucleation" is used rather loosely since this process is evidently different than the formation of nucleating droplets of a new phase as described by classical nucleation theory.) In some cases, the multiple layers of quad-vdW particles evolve into a multiwall tube geometry (Fig. 9), and in this situation the topological evolution of multisheet layers into a multilayer tube geometry is more complicated.

Recent observations of lipid nanotube formation have provided direct evidence for this layer stacking and opening mechanism of nanotube formation [85(b)], and the emergence of nanotubes from multilayer sheets with a local rectangular symmetry has been directly observed in the formation of $H_2Ti_3O_7$ nanotubes [85(c)]. This geometrically awkward and time-consuming process can be avoided through the introduction of seeds that directly initiate tube

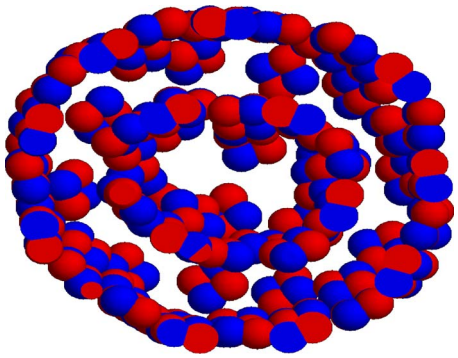

FIG. 9. (Color online) A multiwalled tube formed in square quad-vdW fluid. System conditions: $Q^*=2.0$, $T=1.45$, and $\rho=0.02$.

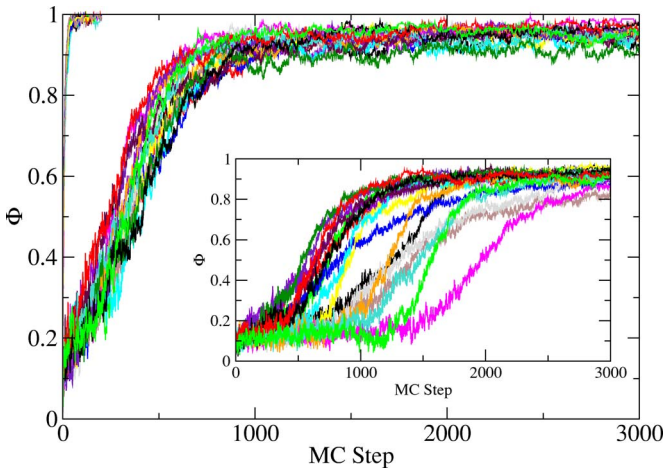

FIG. 10. (Color online) Progress curve $\Phi(t)$ for the quad-vdW fluid. The growth in general becomes more rapid upon cooling, and the amplitude of fluctuations correspondingly grows as the transition temperature is approached. The most rapid growth occurs at $T=1.0$, intermediate rate growth for $T=1.65$, and slow fluctuating growth for $T=1.75$ (inset). System conditions: $Q^*=2.0$, $T=1.0$, 1.65, 1.75, and $\rho=0.001$.

growth. We illustrate this "heterogeneous nucleation" process in the next section for the hexa-vdW fluid where the formation of nanotubes requires some "help" in our simulations.

The geometrical nature of nanotube formation in the quad-vdW particles is considered from a different angle in Fig. 8(b) where we show side and profile views of a fully formed tube in Fig. 7(f). The local rectangular symmetry of the tube is evident, and there is the suggestion of some helicity developing in the tube structure. Note that this emergent helical symmetry is not related to molecular chirality, but derives from the staggering of the particles within the surface to minimize the charge energy. An interplay between the dipole and quadrupole interaction strengths has been suggested to control the angle of this staggering in the case of tubulin [53]. (The emergence of chiral symmetry from nonchiral molecules is discussed by Schnur where he emphasizes the role of particle shape anisotropy in the emergence of chirality in self-assembled nanotubes [13].) We remark that tubulin forms nanotubes with a similar rectangular symmetry [35] as the simulated structures in Fig. 8 and that the general tendency to form helical cylinders is consistent with Crick and Watson's equivalence arguments [39]. Next, we focus on the dynamics of the two-dimensional polymerization process in the quad-vdW model.

Figure 10 shows the progress curves $\Phi(t)$ for the quad-vdW fluid for a relatively deep, moderate, and shallow temperature quench. We see that the rate of assembly becomes more rapid for T increasingly below a characteristic instability range (the precise value of the thermodynamic transition temperature is hard to determine due to our limited system size and the presence of large fluctuation effects, which we discuss below.) This same trend was found for the SF—the stronger the thermodynamic driving force, the more rapid the assembly. Currently, there is no theory that quantitatively explains this trend which seems to apply to self-assembling systems broadly. We also observe that the amplitude of the fluctuations increases as the transition temperature is approached; again, this is similar to the SF and this also seems to be a generic property of self-assembling particle systems. The feature in Fig. 10 which is quite distinct from the SF is the appreciable fluctuations in the time at which the polymerization process initiates, the effect being especially large for shallow quench depths (see the inset to Fig. 10). Such large fluctuation effects in the time at which ordering initiates are characteristic of supercooled liquids where the crystallization transition is a first-order phase transition and, correspondingly, Zhang and Glotzer [57] have agued that the "hysteresis effects" (dependence of nominal thermodynamic properties on the heating and cooling history) found when calculating the specific heat of multifunctionally assembling fluid implies that this kind of transition is first order. Moreover, DiMarzio and Guttman [87,88] have developed a theory of two-dimensional polymerization that accords with this suggestion. In our view, the question of transition order in self-assembling random surfaces should remain open until these systems are studied more carefully. Some aspects of the assembly seem to resemble the SF, while others seem to resemble a kind of "crystallization." At any rate, the large fluctuations in the "nucleation time" t_N explain why it is difficult to obtain well-equilibrated estimates of thermodynamic properties and why calculations made for fixed, albeit long, computational times are apt to exhibit "hysteresis" effects [57].

It is important to appreciate that these fluctuation effects in the assembly process are more than a computational nuisance. Fluctuations in t_N are frequently encountered in the self-assembly of biological systems and have been particularly well studied in the case of sickle cell hemoglobin fiber formation where they have direct significance for the disease expression [89].

The rather large fluctuations in t_N are enhanced by the relatively small system size of our simulations. For larger systems, the transition should become sharper and more reproducible as the probability of having a large number of seeds form after a short time becomes larger for any given run. On the other hand, the self-assembly of many real biological systems often occurs under conditions of small system size and confinement (e.g., the interior of a cell or a cell organelle), so these fluctuation effects have appreciable independent interest for studying self-assembly in biological systems, and we further consider these fluctuation effects and how to control them further in the next section.

Measurements on synthetic fiber forming molecules under bulk solution conditions seem to exhibit rather sharply defined self-assembly transitions, and numerous self-assembling systems have been found to characteristically exhibit the same Arrhenius temperature dependence for the critical concentration [65,66,68] of self-assembly as found for the SF [50]. This suggests to us that that this Arrhenius concentration dependence of the transition curves should also hold for the quad-vdW model (and for the hex-vdW fluid model described in the next section) for large systems, despite our current difficulty of quantitatively determining the self-assembly transition temperature in our simulations. More generally, we suggest that the same thermodynamic

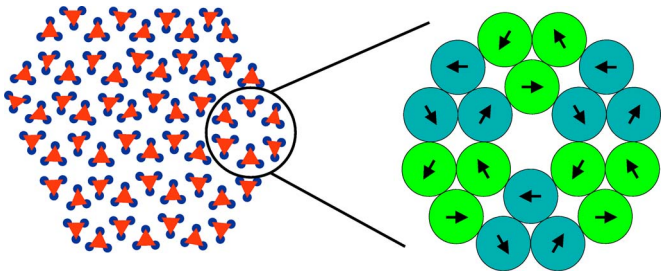

FIG. 11. (Color online) Self-assembled random surfaces formed in the hex-vdW fluid. System conditions: $\mu^*=6.0$, $T=7.75$, and $\rho=0.001$.

analysis that we developed for describing self-assembly in the SF model should also be applicable to self-assembling systems broadly. The validity of this suggestion remains to be checked.

C. Hexapole fluid with van der Waals interaction

Many naturally occurring structures that form by self-assembly exhibit threefold, fivefold, and even higher-order discrete rotational symmetries. We next introduce a minimal fluid model of the multipole type (hex-vdW model) that gives some insight into the origin of these growth forms. As described above, we obtain a simple potential model involving a threefold rotational symmetry by placing SF particles at the vertices of an equilateral triangle in a head-to-tail configuration so that all particles retain their equivalence of interaction.

Upon lowering temperature in the hex-vdW generalization of the SF (interaction parameters are the same as those in Sec. III A), we observe a propensity for self-assembly into random surfaces (see Fig. 11). As expected, these random surfaces exhibit a threefold local symmetry deriving from the symmetry of the hex-vdW particles. Within these sheets, there is a tendency for the + and − lobes of the hex-vdW particle potential to form closed-ring dipolar paths (see the inset to Fig. 11). These observations provide a direct generalization of our previous findings for the quad-vdW fluid where instead the twofold discrete rotational symmetry of the particle potential encoded the formation of random surfaces with a local rectangular structure rather than hexagonal (see Fig. 11). In addition to random surfaces, however, we also observe the spontaneous formation of hollow icosahedral structures with remarkable similarities to viral capsids and the *coexistence* of these structures with open random surfaces [3,43–47]. Figure 12 shows an example of one of these hollow icosahedral structures, which includes a cross-sectional view that reveals its hollow interior. In this series of images, we also depict this structure in terms of the primitive triangles defining the hex-vdW particles. Notably, each particle exhibits "equivalent interactions" and fulfills the formal requirements of Crick and Watson [39].

The formation of icosahedral shells illustrates a new phenomenon regarding how particle symmetry encodes information about the geometry of structures that form by self-organization. In addition to the evident threefold symmetry of the icosahedron faces, an icosahedral shell is characterized by 12 *fivefold* symmetry axes about the vertices of the icosahedron. How did this symmetry arise which is not shared by the single-particle potential? The answer to this question becomes apparent by following the course of the self-assembly process. In the case of the formation of an open hexagonal sheet, the growth pattern is nucleated through the formation of a *hexagonal symmetry seed* composed of six hex-vdW particles in a planar configuration (Fig. 13), while the icosahedral shell is nucleated by the formation of a *pentagonal symmetry seed* having a fivefold symmetry [90]. These fundamental "seed" structures are shown in Fig. 13. Evidently, both the symmetries of the hex-vdW particles and the seeds they form are preserved in the self-assembled structure. The pentagonal seeds (inset to Fig. 14) form from the hex-vdW particles by tilting their orientation with respect to their basal plane, yielding a lower potential energy per particle than for five hex-vdW particles in an 'unsatisfied' flat configuration. The potential energies of the particles within an idealized growing icosahedral sheet and a flat hexagonal sheet are shown in Fig. 14. (Shape fluctuations in the shell and open-sheet structures will change these energies somewhat, but the overall energy trends should be preserved.). Figure 14 shows a progressive decrease of the potential energy per particle for an icosahedral shell grown by progressively adding particles to the edge of the structure until the icosahedral shell is completed and for a hexagonal sheet where each additional particle is placed in a position of lowest potential energy at each step of the assembly of these idealized structures. The energy per particle for the artificially grown icosahedral shell starts a little higher than the hexagonal sheet, but it drops sharply when the pentagon becomes completed, whereupon the potential energy per particle becomes rather slowly varying

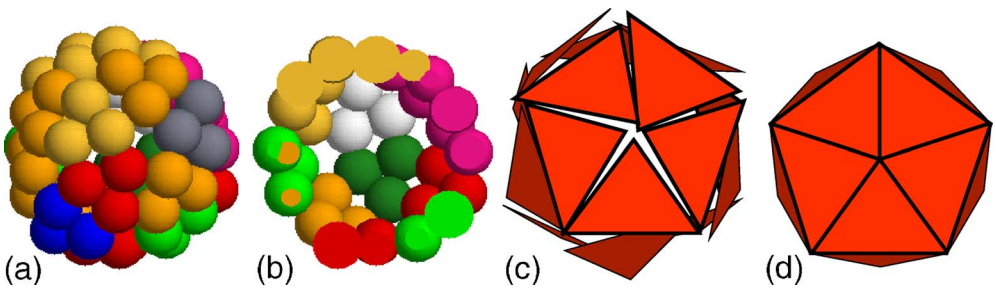

FIG. 12. (Color online) Self-assembled icosahedral shells formed in the hex-vdW fluid. (a) Icosahedron formed from triangular clusters of SF particles, (b) slice through icosahedron revealing cluster interior, (c) representation of icosahedron emphasizing position of faces of triangular particles composing the cluster, and (d) ideal icosahedron. System conditions: $\mu^*=6.0$, $T=7.75$, and $\rho=0.001$.

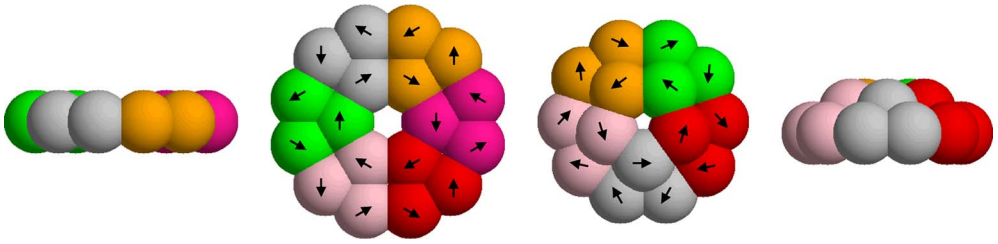

FIG. 13. (Color online) Formation of hexagonal and pentagonal seeds in the hex-vdW fluid (HF). Left images show side and top view of the hexagonal seed, while the right images indicate side and top views of the pentagonal seed. Note that the hex-vdW particles tilt out of the plane to create a surface of near-constant mean curvature.

with the addition of further particles. The potential energy per particle for the hexagon likewise "sticks" to a relatively constant value after the hexagon has finally formed. These results indicate that the energetic driving force can change during the course of assembly and we can expect the formation of certain "magic number" clusters that are especially stable and that can exist in dynamic equilibrium with other cluster geometries having distinct symmetries. If these structures are involved in the self-assembly of some larger structure, then the resulting structures naturally exhibit a quasiequivalent structure containing different local potential environments within the assembly at equilibrium. Notably, this mechanism for quasiequivalent self-assembly *does not require the existence of molecular switches*. The general tendency to form relatively stable pentagonal and hexagonal clusters also accounts for polymorphic growth under nonequilibrium growth conditions (strong thermodynamic driving force) where such structures naturally serve as "seeds" to subsequent growth [54].

The relative similarity of the potential energies per particle in the pentamer and hexamer clusters indicated in Fig. 14 means that it should be possible to *tune* the relative populations of these clusters through varying the dielectric constant and other solution parameters that influence the interparticle interaction strength if these systems are in equilibrium. In conformity with our modeling, it has been found that the relative concentration of pentamer and hexamer units can indeed be reversibly tuned by varying solvent conditions [42,45,54,91]. It might be possible to tune the capsid geometry (e.g., triangulation number) by varying the population of these "capsomere" species in a large-scale simulation by correspondingly tuning of the intermolecular potential parameters to emulate the structures of specific quasiequivalent ($T \neq 1$) viral capsid structures [3]. We infer from the prevalence of quasiequivalent capsid organization in active viruses that we are dealing with dynamic structures formed under *near-thermodynamic equilibrium* conditions. Equilibrium is required for the clusters to rearrange their configuration to explore lower-energy particle configurations to find unique energy-minimizing structures as envisioned by Caspar and Klug [1,3].

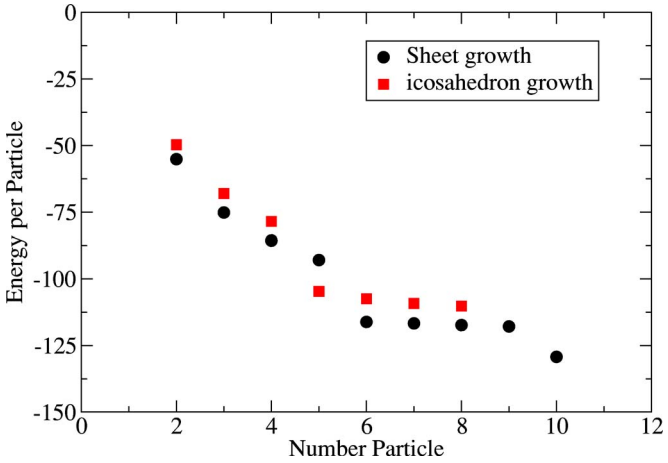

FIG. 14. (Color online) Energy per particle in the sequential ("assembly-line") formation of hexagonal sheets and icosahedral shells in the hex-vdW fluid. System conditions: $T=7.85$, $\mu^*=6.0$, and $\rho=0.001$.

An interesting recent attempt at explaining the prevalence of quasiequivalent structures in spherical viruses was made by Bruinsma and coworkers [46,47]. They start from the assumption that a *fully assembled* virus can be modeled by placing idealized circular disks on a sphere where the disk diameter is varied to model the hexamers and pentamers of the capsid shell. In particular, they prescribe the relative diameters of these disks to equal 0.88, which is remarkably compatible with our simulation estimates of the hexagon-pentagon diameter ratio of 0.88. (Our estimate of this ratio assumes that the SF particles within the hexapole particles have a diameter set by the position of the minimum in the SF particle interaction potential [50] and that the diameter of the pentamer and hexamer is determined by a cylinder that just encloses these model capsomere structures.) Bruinsma and co-workers [46] further assume the existence of equilibrium in the interconversion of the disk structures representing the hexagons and pentagons so that the population of these species is governed by a Boltzmann distribution with an energy E related to the difference in the potential energies between these structures. The most important finding of this work is that quasiequivalent structures only occur when E is sufficiently small so that the capsomeres can feely interconvert. Increasing the dipolar energy in our model leads to an increase in the magnitude of E in the hexapole model so that we would naturally expect a prevalence for the formation of pentagons for large values of the dipolar energy and to deviations from quasiequivalence if our model is combined with the modeling of Bruinsma and co-workers [46]. Correspondingly, there have indeed been observations that certain viruses (polyoma and certain wart viruses) exclusively form assemblies from pentagonal capsomeres, thereby leading to exceptions to the quasiequivalent pattern of viral capsid assembly [42]. Such exceptions are rare, but understandable.

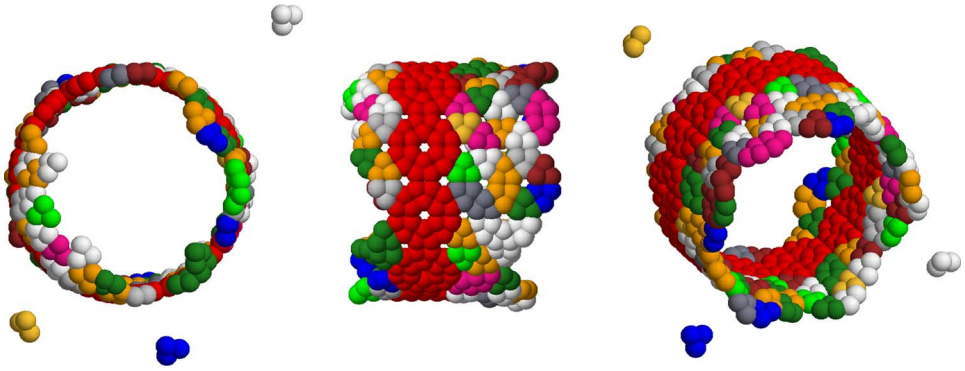

FIG. 15. (Color online) Seeded nanotube formation in the hex-vdW fluid. The image shows from left to right the end-on view, side view, and profile view of the growing tube. System conditions: $T=7.85$, $\mu^*=6.0$, and $\rho=0.001$.

The formation of particle clusters having a fivefold symmetry is not a phenomenon unique to virus capsid formation. The formation of structures having this symmetry is also prevalent in supercooled liquids where icosahedral clusters naturally occur in even simple fluids at low temperatures as the particles evolve towards their lowest-energy local particle configurations [92]. Of course, the fivefold symmetry of these clusters is not compatible with the long-range translational order of bulk crystals (and the acceptable symmetries of the space groups describing crystals). The presence of such structures in cooled liquids can lead to an energetically frustrated and characteristically slow dynamical evolution because of the slow rate of interconversion of these relatively low-energy particle packing configurations into configurations that are representative of a disordered fluid. A frustrated dynamics should also be characteristic of self-assembling systems due to the long residence times of the particles within the dynamic clusters, so we can expect to find many commonalities between the dynamics of self-assembling and glass-forming particle systems [83,84].

In addition to observations of an admixture of hollow icosahedral capsid shells and hexagonal sheets in solutions of capsid-forming proteins *in vitro* [93,94], spherocylindrical viral structures having a morphology similar to carbon nanotubes have also been observed experimentally [77]. While tubular structures with a hexagonal local symmetry do not seem to naturally arise in the hex-vdW model under the conditions we simulated, we can readily generate such structures through the introduction of an appropriate *seed*. In the next section, we discuss how seeding alters the nature of the self-assembly process.

D. Controlling self-assembly with seeds

Inserting seeds of specific symmetry provides an important source of control over the geometry and growth kinetics of self-assembly. Seeding also provides a way of imposing growth symmetries that are not shared by the potential of the assembling particles. It is well known that this *templating process* [95(a),96] is utilized by many biological systems to regulate self-assembly into unique or nearly unique growth forms and this templating must also be of crucial importance for controlling polymorphism in synthetic nanofabrication.

Figure 15 illustrates the growth of a hollow cylinder nucleated from a seed having the form of a ring of (red) hexagons formed from hex-vdW fluid particles. [Our choice of seed structure is motivated by the seeding of microtubule growth by the ring structures assembled from γ-tubulin rings positioned on the centrosome [35(b),35(c)].] We observe from Fig. 15 that this heterogeneous nucleation process leads to the *propagating growth* of a cylinder having a threefold local symmetry, a structure that otherwise does not readily form under the thermodynamic conditions of our simulation. As before, this structure reflects the local symmetries of the assembling particles and the symmetry property imposed by the seed (the near continuous rotational symmetry about the tube axis). The difference here is that the symmetry of the seed is *imposed artificially* rather than by having the seed form itself through a rare nucleation event. We also found that making the seed anisotropic (by turning off the dipole interaction of the two hex-vdW particles on one side of the hexagon ring seed in Fig. 15) leads to *directional growth* along the direction in which the seed dipolar interactions were preserved. An example of a growth morphology generated by this process is shown in Fig. 16. "Polarized growth" of this kind is characteristic of many biological self-assembly processes such as microtubule growth emanating from the centrosome in the course of mitosis [36]. Directed growth dynamics is again a direct consequence of "imprinting" the symmetry properties of the seed particle onto the self-assembled structure. This type of imprinting process is

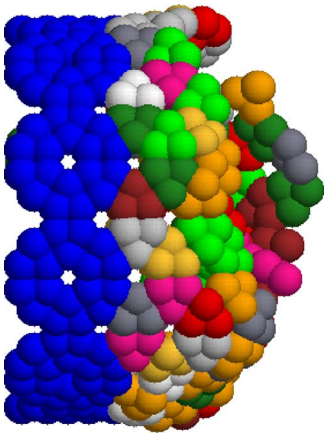

FIG. 16. (Color online) Seeded nanotube formation in the hex-vdW fluid with anisotropic seed. The ring seed is composed of hexagonal "capsomeres" composed of hex-vdW subparticles as in Fig. 15, but only simple LJ particles are incorporated into the left side of the ring seed. Self-assembly growth is "polar" with this ring seed. System conditions: $T=7.85$, $\mu^*=6.0$, and $\rho=0.001$.

probably a significant factor in the templating of inorganic crystalline forms by complex organic self-assembled structures that characterizes the growth forms of many simple organisms [95(b)].

It should also be possible to control the helicity ("chirality") of the tubular assemblies to some degree through seeding, but the pitch that we could achieve by such a procedure must be limited by the energetic cost of the distortions required by imprinting this structure. Although we do not pursue this generalization here, this "chiral seeding" is an obvious approach to controlling the chirality of carbon nanotubes [97(a)] and other organic and inorganic nanotube structures.

γ-tubulin forms a lock-washer-shaped ring structure [35(b),35(c)] that may act in the fashion by regulating the helicity of microtubules (which seems to exhibit variable helicity according to its preparation) that grow from the centrosome during cell division.

As an aside, we note that we had some difficulty growing long tubes having hexagonal local symmetry due the insertion of pentamer hex-vdW clusters in the course of growth. Once these defect structures are introduced into the tube, there is a general tendency for the tube to pinch-off to form a closed surface. This effect has also been observed in molecular dynamics simulations at the growth of single wall nanotubes [97(c)]. By Euler's theorem, the resulting irregularly shaped closed surfaces have *exactly* 12 pentagonal vertices [98], as in the case of perfect icosahedral shells. When this pinching-off effect is very strong and occurs symmetrically along the tube periphery, it apparently can lead to the formation of *conelike* closed capsule structures. (These structures are commonly observed in fullerene molecules and in the viral core capsids of HIV and retroviruses of disease interest [77,99]. The physical factors that control the organization and stability of these asymmetric core capsid structures are important because the disruption of these structures has been found to significantly influence virus infectivity [77].) Interestingly, these cone-shaped capsules are predicted to exhibit quantized cone angles associated with the allowable positioning of the pentagonal "defects" in the shell and these exotic structures have been experimentally observed in viruses and there fullerene "analogs" [77,97(a)].

The introduction of an artificial seed also has a dramatic influence on the evolution of the self-assembly process. The growth kinetics without the seed exhibited intense fluctuations in the time for which assembly initiates from simulation to simulation, as discussed in Secs. III C and II D. Eliminating the requirement for homogeneous nucleation of a seed structure in the growth dynamics leads to a self-assembly growth process that is much more reproducible. Moreover, seeding can dramatically reduce the average time required for growth initiation and thus can reduce the time required for self-assembly. We next discuss the origin of the fluctuations in the initiation time, and we then show how these fluctuation effects can be controlled with seeds.

The fluctuations in the initiation time occurring in the quad-vdW and hex-vdW models can be traced to the formation of hexagonal and pentagonal seeds, which are especially rare events close to the thermodynamic transition temperature where the energetic driving forces are weak. (Recent measurements have been able to directly observe quasiplanar nuclei in protein crystallization [100], but otherwise observations of seed structures in protein self-assembly are quite rare.) Under these conditions, there are large fluctuations in the nucleation timescale. We illustrate this general phenomenon in Fig. 17(a) where $\Phi(t)$ for the particular case of the hex-vdW fluid is shown for temperatures close, moderately below, and far below T_Φ. As noted before, the fluctuations become larger for smaller quench depths, while the rate of self-assembly increases with quench depth. Nucleation events are apparently more sharply defined in the quad-vdW model than for the hex-vdW fluid, an effect no doubt related to the larger number of particles needed for the formation of the hex-vdW fluid seeds.

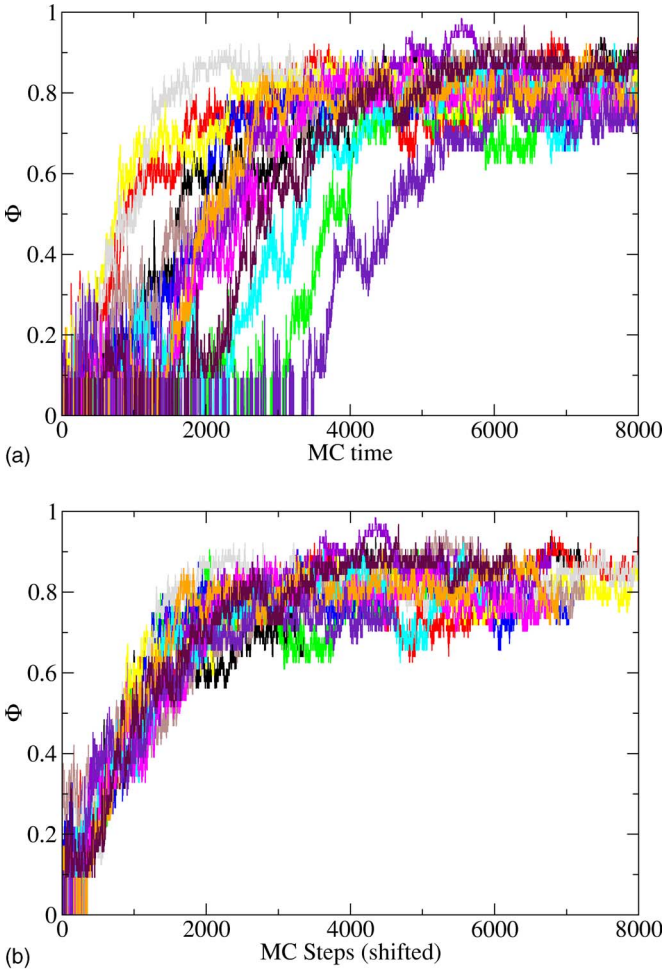

FIG. 17. (Color online) Progress curves $\Phi(t)$ for the hex-vdW fluid. The top image shows the large fluctuations that occur in nucleation time t_N and in the magnitude of $\Phi(t)$ close to the thermodynamic transition. The bottom image shows the result of time-shifting $[\Phi(t) \rightarrow \Phi(t-t_N)]$ the curves in the top image. System conditions are identical for each run: $\mu^* = 6.0$, $T = 7.85$, and $\rho = 0.001$.

It is apparent that all the $\Phi(t)$ curves in Fig. 17(b) grow in a similar qualitative fashion once nucleation has initiated. The main source of variability is then the nucleation time t_N itself. We can gain some insight into this general property of the $\Phi(t)$ curves by shifting the time coordinate to a time t relative to t_N. The time-shifted $\Phi(t-t_N)$ data nearly superimpose, and a similar procedure also works for $\Phi(t)$ data for the well-studied case of the self-assembly of sickle cell hemo-

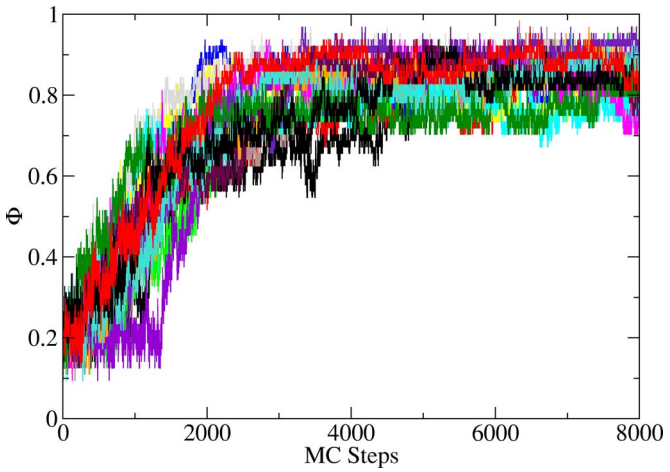

FIG. 18. (Color online) Progress curves $\Phi(t)$ for the hex-vdW fluid with a seed. System conditions are identical to those for Fig. 17, except that a hexagonal seed (see Fig. 13) has been incorporated. System conditions: $\mu^*=6.0$, $T=7.85$, and $\rho=0.001$.

globin protein fibers under confinement [solution volume $\sim O(10^{-15}-10^{-16}\ \mathrm{m}^3)$] conditions [101]. By performing many simulations and averaging the results, we can determine the average rate of these inherently stochastic t_N fluctuations [102,103]. This procedure, which has been performed in the case of sickle cell hemoglobin [89,101,102], requires hundreds of simulations to acquire good statistics, and this ambitious task is avoided in the present paper. Next, we consider how the introduction of a seed influences the kinetics of self-assembly.

Figure 18 shows an example of how the introduction of an artificial seed modifies growth kinetics under conditions where intense fluctuations were formerly exhibited (see Fig. 10). We see that by eliminating the requirement for homogeneous nucleation of a seed, we obtain $\Phi(t)$ curves that are much more reproducible. (Seedlike structures that form at the early stage of growth due to homogeneous nucleation evidently compete with the artificial seed, leading to some residual fluctuations at short times, but this is a secondary effect.) Seeding generally reduces the average time for growth to initiate and thus can substantially reduce the overall time required for self-assembly. After seeding the $\Phi(t)$ curves for the quad-vdW and hex-vdW models are reasonably smooth and do not require any time shifting to achieve superposition. Moreover, the qualitative shape of the $\Phi(t)$ curves with the seeded growth then resembles the assembly kinetics of the SF model where nucleation effects are not apparently operative. Thus, seeding is apparently a powerful means of regulating both the structure and kinetics of assembly structures involving two-dimensional polymerization.

IV. CONCLUSIONS

We have sought to understand how the symmetry properties of the particle potential encodes information about the geometry of self-assembled structures and to determine primary factors that influence the kinetics of the self-assembly. Our principle motivation for this work is to provide guidance in the fabrication of synthetic self-assembling systems. Although our treatment has been restricted to potentials combining directional (multipole) interactions with isotropic van der Waals interactions, similar effects can be expected to arise from other highly directional interactions [9] (hydrogen bonding, hydrophobic interactions, π-π interactions of aromatic species, metal chelation, etc.) in competition with van der Waals interactions. Anisotropic contributions to the interaction potential arising from particle shape anisotropy are also basic to understanding real self-assembling systems. On the other hand, biological molecules characteristically have large Coulombic, dipolar, and multipole interactions, so this class of potentials offers a reasonable starting point for modeling certain broad trends in biological self-assembly and for ascertaining factors of practical significance in controlling synthetic self-assembly in future nanofabrication applications. The long-range character of these interactions would make shape anisotropy contributions to the interparticle interaction weaker than in fluids with short-range interactions.

In previous work, we extensively studied the Stockmayer fluid as prototypical model of molecular self-assembly. In this model, we observe the formation of linear polymer chains that exist in dynamic equilibrium and which have well-defined equilibrium properties that are well described by the theory of equilibrium polymerization [50,58]. The potential of this model is characterized by a continuous rotational symmetry about the dipole axis [50], which allows us to continuously tune the extent of polymerization Φ, chain length L, and other thermodynamic properties as a function of temperature. The organization and disordering processes are readily reversible [50]. This model of self-assembly provides a reference point for comparison to our new results for self-assembly in fluids where the particle potential has a discrete rotational symmetry and where many new effects emerge in association with this symmetry change.

The hex-vdW fluid is constructed from the same Stockmayer fluid particles, but we array the particles at the vertices of a triangle to create composite particles with a threefold rotational symmetry. Unexpectedly, we found that the discrete rotational symmetry of the hex-vdW fluid particle potential *qualitatively* changes the kinetics, as well as the structures that form upon self-assembly. The self-assembly transition exhibits large fluctuation effects reminiscent of a first-order phase transition, and it becomes difficult to estimate thermodynamic properties from simulations. In particular, the progress curves $\Phi(t)$ describing the organizational kinetics become dependent on an essentially random "nucleation time" t_N at which self-assembly initiates. We also find that the form of the self-assembly is quite sensitive to the geometry of the seeds that arise in the course of growth and to seed particles added before assembly has initiated. As a consequence, the resulting self-assembled structures tend to be polymorphic if the organizational process is not subjected to control through the introduction of artificial seeds [54]. On the other hand, it is possible to generate essentially *unique* structures and to control the fluctuations in the organization time through the introduction of seeds to direct the growth. This templating effect [104] and the observation of stochastic evolution arising from fluctuations generated by relatively rare nucleation events are characteristic features of biological

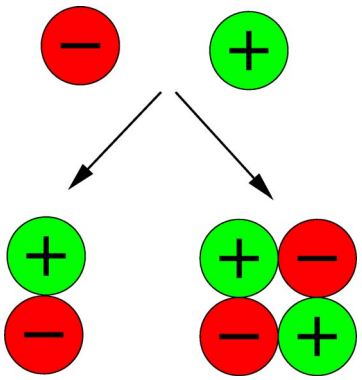

FIG. 19. (Color online) Self-assembly of spherical ions (monopoles) into particles with dipolar and quadrupole interactions. These structures in turn become the assembling elements at the next level of self-assembly.

self-assembly, and the quad-vdW and hex-vdW models provide a laboratory for studying these fundamental effects.

The self-assembly of random surface structures in both the quadrupole–van derWaals and hexapole–van der Waals fluids provides clear examples of how the local symmetries of the particle potential encode information about the self-assembly organization, thus validating our central hypothesis that the particle point-group symmetries tend to be preserved in the particle assemblies. In particular, the quad-vdW fluid led to the formation of random surfaces with a local rectangular symmetry, while the hex-vdW fluid led to two-dimensional polymer surfaces having a three fold local symmetry. Curiously, the icosahedral shells that form in the hex-vdW fluid exhibit symmetries that are not possessed by the assembling particles. The formation of these hollow shells occurs through the formation of low-energy pentagonal seeds in the course of the early assembly, and the curvature of this structure causes the assembly to evolve into completed shells having an icosahedral symmetry in which both the symmetries of the hex-vdW particles and the seeds that form from them are encoded. Numerous important biological structures (virus capsid shells and the core capsid structures of complex viruses such as HIV, clathrin, etc.) involve an organization of closed surfaces built up from a combination of similar hexagonal and pentagonal structural elements, and this simple model gives some insight into the nature of this growth process. For example, we find that no molecular switch is required for the pentagonal and hexagonal structures of quasiequivalent virus structures to form in our model, although this does not deny the existence of these structures or their functioning in real viral capsid assembly, as originally conceived by Caspar and Klug [3].

Although the matter is challenging computationally, charged and dipolar particles characteristically exhibit a hierarchy of self-assembled structures. Recent works [54,55] have shown that even simple charged spheres will organize into dipolar and multipolar configurations to reduce their local charge energy (see Fig. 19). Square quadrupole configurations are energetically favored on an energy per particle basis if the particles have the same size and valence, but dipolar or linear quadrupole geometries can have lower energies when there is a particle size or valence asymmetry. These ionic clusters, in turn, can be viewed as forming the structural elements in our simulations. In this way, it should be possible to build up complex patterns having symmetries quite distinct from the primary particles. Apparently subtle differences in the size and electrostatic or other interaction characteristics can impose themselves onto the large-scale symmetry of the resulting self-assembly. Further computational investigations will be needed to understand the general principles that underlie these additional factors that influence the geometry and nature of molecular self-assembly. Real particle clusters involve a superposition of charge, dipolar, quadrupolar, and higher-order polar interactions, in addition to shape anisotropy and other anisotropies in the interaction potential. Evidently, it should be possible to trigger transitions between the various types of self-assembled structures by varying the relative strengths of these interactions so that there is a change in dominant symmetry in the self-assembly. Changes of this kind could well explain the transformation from a nanotube to a ring morphology in microtubules exposed to certain drugs and proteins associated with viral infection [105].

ACKNOWLEDGMENT

K.V.W. would like to thank the National Research Council and NIST for support.

[1] A. Klug, Proc. R. Soc. London, Ser. A **348**, 167 (1994).
[2] F. Oosawa and S. Asakura, *Thermodynamics of the Polymerization of Protein* (Academic Press, New York, 1975).
[3] D. L. D. Caspar and A. Klug, Cold Spring Harbor Symp. Quant. Biol. **27**, 1 (1962). See also D. L. D. Caspar, Biophys. J. **32**, 103 (1980); L. Makowski, *ibid.* **74**, 534 (1998); J. E. Johnson and J. A. Speir, J. Mol. Biol. **269**, 665 (1997).
[4] D. Philp and J. F. Stoddart, Angew. Chem., Int. Ed. Engl. **35**, 1155 (1996).
[5] J. S. Moore, Curr. Opin. Colloid Interface Sci. **4**, 108 (1999).
[6] J. M. Lehn, *Supramolecular Chemistry* (VCH, Weinheim, 1995).
[7] A. P. Alivisatos, K. P. Johnsson, X. G. Peng, T. E. Wilson, C. J. Loweth, M. P. Bruchez, and P. G. Schultz, Nature (London) **382**, 609 (1996).
[8] S. A. Jeneke and X. L. Chen, Science **283**, 372 (1999).
[9] L. Brunsveld, B. J. B. Folmer, E. W. Meijer, and R. P. Sijbesma, Chem. Rev. (Washington, D.C.) **101**, 4071 (2001).
[10] B. J. de Gans, S. Wiegand, E. R. Zubarev, and S. I. Stupp, J. Phys. Chem. B **106**, 9730 (2002).
[11] S. I. Stupp, S. Son, H. C. Lin, and L. S. Li, Science **259**, 59 (1993); S. I. Stupp, V. LeBonheur, K. Walker, L. S. Li, K. E. Huggins, M. Keser, and A. Amstutz, *ibid.* **276**, 384 (1997).
[12] C. A. Mirkin *et al.*, Nature (London) **382**, 607 (1996).

[13] J. Schnur, Science **262**, 1669 (1993).
[14] M. R. Ghadiri *et al.*, Nature (London) **366**, 324 (1993). See also J.-H. Furhop and W. Helfrisch, Chem. Rev. (Washington, D.C.) **93**, 1565 (1993).
[15] D. S. Lawrence, T. Jiang, and M. Levelt, Chem. Rev. (Washington, D.C.) **95**, 2229 (1995).
[16] F. Oosawa and S. Asakura, *Thermodynamics of the Polymerization of Protein* (Academic Press, New York, 1975).
[17] C. Freiden, Proc. Natl. Acad. Sci. U.S.A. **80**, 6513 (1983).
[18] T. D. Pollard and J. A. Cooper, Annu. Rev. Biochem. **55**, 987 (1986).
[19] P. S. Niranjan, P. B. Yim, J. G. Forbes, S. C. Greer, J. Dudowicz, K. F. Freed, and J. F. Douglas, J. Chem. Phys. **119**, 4070 (2003).
[20] H.-C. Chang, T.-L. Lin, and G.-G. Chang, Biophys. J. **78**, 2070 (2000).
[21] H. Fraenkel-Conrat and R. C. Williams, Proc. Natl. Acad. Sci. U.S.A. **41**, 690 (1955).
[22] P. J. G. Butler, J. Gen. Virol. **65**, 253 (1984). See also [94].
[23] B. Maddox, *Rosalind Franklin: The Dark Lady of DNA* (Harper Collins, New York, 2002), pp. 249–252. This work discusses the novelty of the concept of "structural equivalence" that was derived from Rosalind Franklin's studies of TMV and the ramifications of this radical idea for her continued funding.
[24] J. Hofrichter, P. D. Ross, and W. A. Eaton, Proc. Natl. Acad. Sci. U.S.A. **71**, 4864 (1974).
[25] F. A. Ferrone, J. Hofrichter, and W. A. Eaton, J. Mol. Biol. **183**, 553 (1986). See Refs. [97,101,102].
[26] E. Samuel, E. D. Salman, and R. W. Briehl, Nature (London) **345**, 833 (1990).
[27] O. Gaiken and P. G. Vekilov, J. Mol. Biol. **336**, 43 (2004).
[28] G. Forgacs, S. A. Newman, B. Hinner, C. W. Maier, and E. Sackmann, Biophys. J. **84**, 1272 (2003).
[29] D. Waugh, J. Am. Chem. Soc. **68**, 247 (1946).
[30] E. Koo, P. T. Lansbury, Jr., and J. W. Kelly, Proc. Natl. Acad. Sci. U.S.A. **96**, 9989 (1999).
[31] L.-W. Jin *et al.*, Proc. Natl. Acad. Sci. U.S.A. **101**, 15294 (2003). See also M. R. H. Krebs *et al.*, *ibid.* **101**, 14420 (2004).
[32] D. M. Walsh *et al.*, J. Biol. Chem. **274**, 25945 (1999); A. Lomakin *et al.*, Proc. Natl. Acad. Sci. U.S.A. **93**, 1125 (1996); **94**, 7942 (1997); C. Valery *et al.*, *ibid.* **100**, 10258 (2003); N. Aripse, H. P. Pollard, and E. Rojas, *ibid.* **90**, 10573 (1993).
[33] P. B. Schiff, J. Fant, and S. B. Horwitz, Nature (London) **277**, 665 (1979); H. P. Erickson, D. W. Taylor, and D. Bram Hill, Proc. Natl. Acad. Sci. U.S.A. **93**, 519 (1996).
[34] T. Mitchison and M. Kirschner, Nature (London) **312**, 232 (1984); **312**, 237 (1984).
[35] (a) L. A. Amos and W. Bradshaw, *Molecules of the Cytoskeleton* (McMillan, London, 1991), Chap. 7; (b) M. Moritz, M. B. Braunfeld, V. Guénebaut, J. Heuser, and D. A. Agard, Nat. Cell Biol. **2**, 365 (2000); H. P. Erickson, *ibid.* **2**, E93 (2000).
[36] W. A. Voter and H. P. Erickson, J. Biol. Chem. **259**, 10430 (1984).
[37] D. K. Fygenson, E. Braun, and A. Libchaber, Phys. Rev. E **50**, 1579 (1994); H. Flyvbjerg, T. E. Holy, and S. Leibler, *ibid.* **54**, 5538 (1996).
[38] K. F. Freed, Phys. Rev. E **66**, 061916 (2002).
[39] F. H. C. Crick and J. D. Watson, Nature (London) **177**, 473 (1956).
[40] J. B. Bancroft, *Advances in Virus Research* (Academic, New York, 1970).
[41] A. Klug, Nature (London) **303**, 378 (1983).
[42] N. A. Kiselev and A. Klug, J. Mol. Biol. **40**, 155 (1969) (see Fig. 10 of this work); I. Rayment, T. S. Baker, D. L. D. Caspar, and W. T. Murakami, Nature (London) **295**, 110 (1982); K. W. Adolph and P. J. G. Butler, J. Mol. Biol. **88**, 327 (1974).
[43] P. E. Privelige, D. Thomas, and J. King, Biophys. J. **64**, 824 (1993).
[44] T. S. Baker, N. H. Olson, and S. D. Fuller, Microbiol. Mol. Biol. Rev. **63**, 862 (1999); M. G. Rossmann and J. E. Johnson, Annu. Rev. Biochem. **58**, 583 (1989).
[45] A. Zlotnik, J. Mol. Biol. **241**, 59 (1994); D. Endres and A. Zlotnick, Biophys. J. **83**, 1217 (2002); A. Zlotnik, Proc. Natl. Acad. Sci. U.S.A. **101**, 15549 (2004). For a discussion of the importance of understanding virus assembly in relation to treating aids; see H. R. Gelderblom, AIDS **5**, 617 (1991).
[46] R. F. Bruinsma, W. M. Gelbart, D. Reguera, J. Rudnick, and R. Zandi, Phys. Rev. Lett. **90**, 248101 (2003). See also C. J. Marzec and L. A. Day, Biophys. J. **65**, 2559 (1993).
[47] R. Zandi, D. Reguera, R. F. Bruinsma, W. M. Gelbart, and J. Rudnick, Proc. Natl. Acad. Sci. U.S.A. **101**, 15556 (2004).
[48] R. Nossal, Traffic **2**, 138 (2001). See also R. A. Crowther, and B. M. F. Pearse, J. Cell Biol. **91**, 790 (1981); F. M. Brodsky, Science **242**, 1396 (1988). Cage structures similar to clathrin arise in intracellular vesicle transport between organelles: K. Matsoka, R. Schekman, L. Orei, and J. E. Heuser, Proc. Natl. Acad. Sci. U.S.A. **98**, 13705 (2001).
[49] D. C. Rapaport (unpublished). See also D. C. Rapaport, J. E. Johnson, and J. Skolnick, Comput. Phys. Commun. **121–122**, 231 (1999).
[50] K. Van Workum and J. F. Douglas, Phys. Rev. E **71**, 031502 (2005). See also J. Dudowicz and K. F. Freed, Phys. Rev. Lett. **92**, 045502 (2004).
[51] J. Staumbaugh, K. Van Workum, and J. F. Douglas, and W. Losert, Phys. Rev. E **72**, 031301 (2005).
[52] K. Van Workum and J. F. Douglas, Macromol. Symp. **227**, 1 (2005); J. F. Douglas and W. K. Van Workum, in Lessons from Simulation Regarding the Control of Self-Assembly, edited by N. Langrana and F. Horkay, MRS Symposia Proceedings (Materials Research Society, in press).
[53] J. Staumbaugh, Ph.D. thesis, University of Maryland, 2004. The raw data from which the dipole moments were calculated were obtained from the protein databank.
[54] D. M. Salunke, D. L. D. Caspar, and R. L. Garcea, Biophys. J. **56**, 887 (1989).
[55] Q. L. Yan, and J. J. de Pablo, Phys. Rev. Lett. **88**, 095504 (2002); J. M. Romero-Enrique, G. Orkoulas, A. Z. Panagiotopoulos, and M. E. Fisher, *ibid.* **85**, 4558 (2000).
[56] J. Tsao *et al.*, Nature (London) **251**, 1456 (1991); A. J. Fisher and J. E. Johnson, *ibid.* **361**, 177 (1993).
[57] Z. Zhang and S. C. Glotzer, Nano Lett. **4**, 1407 (2004); Z. Zhang, M. A. Horsch, M. H. Lamm, and S. C. Glotzer, *ibid.* **3**, 1341 (2003).
[58] (a) J. Dudowicz, K. F. Freed, and J. F. Douglas, J. Chem. Phys. **112**, 1002 (2000); (b) **113**, 434 (2000); (c) **119**, 12645 (2003).
[59] D. J. Mercurio and R. J. Spontak, J. Phys. Chem. B **105**, 2091 (2001).
[60] E. A. Wilder, C. K. Hall, S. A. Khan, and R. J. Spontak,

Langmuir **19**, 6004 (2003).
[61] A. Thierry, C. Straupé, B. Lotz, and J. C. Wittman, Polym. Commun. **31**, 299 (1990).
[62] T. Bauer, R. Thomann, and R. Mülhaupt, Macromolecules **31**, 7651 (1998).
[63] R. K. Fuchs *et al.*, Macromolecules **32**, 8404 (1999).
[64] D. J. Abdallah and R. G. Weiss, Adv. Mater. (Weinheim, Ger.) **12**, 1237 (2000).
[65] P. Terech and R. G. Weiss, Chem. Rev. (Washington, D.C.) **97**, 3133 (1997).
[66] P. Terech, C. Rossat, and F. Volino, J. Colloid Interface Sci. **227**, 363 (2000).
[67] P. Teresch, Ber. Bunsenges. Phys. Chem. **102**, 1630 (1998).
[68] T. Brotin, R. Utermöhlen, F. Fages, H. Bouas-Laurent, and J.-P. Desvergne, J. Chem. Soc., Chem. Commun. **6**, 416 (1991).
[69] F. Placin, M. Colomés, and J.-P. Desvergne, Tetrahedron Lett. **38**, 2665 (1997); F. M. Menger and K. L. Caran, J. Am. Chem. Soc. **122**, 11679 (2000).
[70] A. P. Nowak, V. Breedveld, L. Pakstis, B. Ozbas, D. J. Pine, D. Pochan, and T. J. Deming, Nature (London) **417**, 424 (2002).
[71] J. P. Schneider, D. J. Pochan, B. Ozbas, K. Rajagopal, L. Pakstis, and J. Kretsinger, J. Am. Chem. Soc. **124**, 15030 (2002).
[72] D. J. Pochan, J. P. Schneider, J. Kretsinger, B. Ozbas, K. Rajagopal, and L. Haines, J. Am. Chem. Soc. **125**, 11802 (2003).
[73] M. R. Stapleton, D. J. Tildesley, A. Z. Panagiotopoulos, and N. Quirke, Mol. Simul. **2**, 147 (1989).
[74] B. Smit and C. P. Williams, J. Phys.: Condens. Matter **2**, 4281 (1990).
[75] G. S. Dubey and S. F. O'Shea, Phys. Rev. E **49**, 2175 (1994); S. F. O'Shea, G. S. Dubey, and J. C. Rasaiah, J. Chem. Phys. **107**, 237 (2002).
[76] M. Dijkstra, J. P. Hansen, and P. A. Madden, Phys. Rev. Lett. **75**, 2236 (1995); Phys. Rev. E **55**, 3044 (1997).
[77] B. K. Ganser, S. Lu, V. K. Klishko, J. T. Finch, and W. I. Sundquist, Science **283**, 80 (1999). See also S. Li, C. P. Hill, W. L. Sundquist, and J. T. Finch, Nature (London) **407**, 409 (2000).
[78] J. C. Shelley, G. N. Patey, D. Levesque, and J. J. Weis, Phys. Rev. E **59**, 3065 (1999).
[79] B. Chen and J. I. Siepmann, J. Phys. Chem. B **105**, 11275 (2001).
[80] I. S. Jacobs and C. P. Bean, *Magnetism* (Academic Press, New York, 1963).
[81] M. A. Miller and D. J. Wales, J. Phys. Chem. B **109**, 23109 (2005).
[82] H. B. Lavender, K. A. Iyer, and S. J. Singer, J. Chem. Phys. **101**, 7856 (1994).
[83] S. K. Kumar and J. F. Douglas, Phys. Rev. Lett. **87**, 188301 (2001).
[84] D. Bedrov, G. D. Smith, and J. F. Douglas, Europhys. Lett. **59**, 384 (2002); Polymer **45**, 3961 (2004).
[85] (a) J. F. Douglas, Phys. Rev. E **54**, 2677 (1996); G. S. Murat, and M. Murat, J. Phys. (Paris) **51**, 1415 (1990); (b) V. S. Kulkarni, J. M. Boggs, and R. E. Brown, Biophys. J. **77**, 319 (1999); (c) S. Zhang, L.-M. Peng, Q. Chen, G. H. Du, G. Dawson, and W. Z. Zhou, Phys. Rev. Lett. **91**, 256103 (2003).
[86] C. F. Schmidt *et al.*, Science **259**, 952 (1993).
[87] E. A. DiMarzio and C. M. Guttman, J. Cryst. Growth **57**, 403 (1982).
[88] E. A. Di Marzio, Prog. Polym. Sci. **24**, 329 (1999).
[89] H. Sunnshine, J. Hofrichter, and W. A. Eaton, Nature (London) **275**, 238 (1978); A. Mozzarelli, J. Hofrichter, and W. A. Eaton, Science **237**, 500 (1987). See also [102] and [103].
[90] B. M. Hespenheide, D. C. Jacobs, and M. F. Thorpe, J. Phys.: Condens. Matter **16**, S5055 (2004).
[91] Z. Xie and R. W. Hendrix, J. Mol. Biol. **253**, 74 (1995).
[92] P. J. Steinhardt, D. R. Nelson, and M. Ronchetti, Phys. Rev. B **28**, 784 (1983); D. R. Nelson, *ibid.* **28**, 5515 (1983); H. Jónsson and H. C. Andersen, Phys. Rev. Lett. **60**, 2295 (1988); F. H. Zetterling, M. Dzugutov, and S. I. Simdyankin, *ibid.* **89**, 195701 (2002); M. H. Reichert *et al.*, Nature (London) **408**, 839 (2000).
[93] J. B. Bancroft, C. E. Bracker, and G. W. Wagner, Virology **38**, 324 (1969); J. B. Bancroft, Adv. Virus Res. **19**, 99 (1970).
[94] P. J. G. Butler, Int. Rev. Biochem. **25**, 205 (1979).
[95] (a) Z. Cao and F. A. Ferrone, Biophys. J. **72**, 343 (1997); J. King and S. Casjens, Nature (London) **251**, 112 (1974); (b) H. A. Lwenstam and G. Weiner, *Biomineralization* (Oxford University Press, Oxford, 1989).
[96] A. Klug, Angew. Chem., Int. Ed. Engl. **22**, 565 (1983).
[97] Many elemental systems (S, P, Se, Te, …) exhibit *thermally reversible* equilibrium polymerization where true chemical bonds form rather than physical associations (See Ref. 52 of [58(c)]) and where quantum mechanics governs the symmetry properties of the bonding (*p* orbitals having the symmetry of a dipolar potential, *d* orbitals having the symmetry of the quadrupole potential, and sp^3-hybrid orbitals having the threefold symmetry of the hexapole potential). It is not clear whether the formation of carbon nanotubes and other fullerenes can be described by this kind of equilibrium self-assembly process, but these structures have been found to interconvert upon heating, consistent with this possibility [F. Banhart and P. M. Ajayan, Nature (London) **382**, 433 (1996); M. Endo *et al.*, Nano Lett. **4**, 1451 (2004)]. The geometrical structures of many inorganic and organic nanotubes, including carbon nanotubes, are certainly strikingly similar to their biological "counterparts" found in the organization of viruses and other self-assembled biological structures.J. Charlier, A. DeVita, X. Blasé, and R. Car, Science **275**, 646 (1997).
[98] (a) T. Kanaseki and K. Kadota, J. Cell Biol. **42**, 202 (1969); (b) R. Nossal, and H. Lecar, *Molecular and Cell Biophysics* (Addison-Wesley, New York, 1991), Chap. 5.
[99] (a) B. I. Yakobson and R. E. Smalley, Am. Sci. **85**, 324 (1997); (b) M. Ge and K. Sattler, Chem. Phys. Lett. **220**, 192 (1994).
[100] S. T. Yau and P. G. Vekilov, Nature (London) **406**, 494 (2000).
[101] F. A. Ferrone, J. Hofrichter, W. A. Eaton, and F. A. Ferrone, J. Mol. Biol. **183**, 591 (1985). See Fig. 17 of this work.
[102] J. Hofrichter, J. Mol. Biol. **189**, 553 (1986).
[103] A. Szabo, J. Mol. Biol. **199**, 539 (1988).
[104] M. S. Chapman, Biophys. J. **74**, 639 (1998).
[105] N. R. Watts *et al.*, J. Cell Biol. **150**, 349 (2000).